Systematic molecular dynamics studies of liquid *N*,*N*-dimethylformamide using optimized rigid force fields: Investigation of the thermodynamic, structural, transport and dynamic properties

Michalis Chalaris and Jannis Samios[a)]
University of Athens, Department of Chemistry, Laboratory of Physical Chemistry, Panepistimiopolis 157-71, Athens, Greece

(Received 23 November 1999; accepted 18 February 2000)

The properties of the pure liquid *N*,*N*-dimethylformamide were investigated by means of microcanonical (NVE) and isothermal–isobaric (NPT) molecular dynamics simulation techniques. Previously proposed five- and six-interaction-site optimized potential models (OPLS) were employed to simulate the liquid at different state points and their properties were obtained and discussed. The results obtained have shown that these models, to a higher or lower degree, yield realistic descriptions of the liquid. We have found, however, that a systematic readjustment of the potential parameters is necessary in order to describe the liquid properties more accurately. Thus, a new six-interaction-site OPLS computational model for liquid *N*,*N*-dimethylformamide has been derived. It turns out that this model can describe not only the thermodynamic and structural properties but also the dynamic (single and Debye relaxation) and the transport properties (self-diffusion, shear viscosity) of the system with good accuracy in the entire temperature range at normal pressure. © *2000 American Institute of Physics.* [S0021-9606(00)51218-5]

I. INTRODUCTION

It is well known that amides represent an important class of organic solvents. Furthermore, these organic compounds may be used as model systems for peptides. Consequently, investigating the properties of such molecular systems becomes a very interesting task since it would lead to a more accurate knowledge and thus towards a better understanding of the overall behavior of these systems.

Formamide (FA), *N*-methylformamide (NMF) and *N*,*N*-dimethylformamide (DMF) are the simplest amide compounds with interesting properties. These molecules have large dipole moments and it is expected that in the liquid state the dipole–dipole interactions dominate the intermolecular forces. A consequence of this is presumably that these interactions should form a definitive short range ordering among the molecules. Another important feature of these liquids is that they represent two different classes of solvents. More specifically, FA and NMF are hydrogen bonded solvents at liquid conditions. On the other hand, the liquid DMF is an aprotic dipolar solvent. Therefore, a systematic and comparative investigation of these liquids should lead to a deeper understanding of the role of various type of interactions which are responsible for their properties.

As far as we know, the three above-mentioned pure liquids and their mixtures have been studied thoroughly using several experimental techniques. These studies include various thermodynamic, transport and structural measurements as well as dynamical spectroscopic ones.

Theoretical considerations via computer simulation (CS) studies have also been carried out mainly to study the energetic and structural properties of these liquids.

However, following the literature we can notice that only a limited number of molecular dynamics (MD) simulation studies on such liquids have been reported until the time this work was written. Yasonath and Rao (YR)[1] published the first MD study of pure liquid DMF at room temperature and normal pressure. This work was based on an optimized five-site pairwise additive potential model, proposed by Jorgensen and Swenton (JS)[2,3] in previous Monte Carlo (MC) studies. According to the technical details reported in Ref. 1, that study was based on a very small number of molecules ($N=64$) in the central simulation box. Moreover, the various time correlation functions (CFs) were obtained on the basis of relatively small phase space trajectories which lasted for about 20 ps.

In a subsequent MD treatment, Schoester *et al.*[4] reported results concerning the intermolecular structure of these amides at room temperature. In their study, the molecular interactions were reinvestigated and a new generalized flexible potential model for the three liquids was proposed. In the case of DMF, the corresponding intermolecular potential model, hereafter denoted as the SM model, was represented by six interactions sites with a short range Lennard-Jones (12–6) (LJ) part and a long range Coulombic term. Each methyl group (cis, trans) is approximated as a united interaction site located at the position of the methyl carbon. It is important to notice that the estimation of the potential parameters in that treatment was based on a bimolecular optimized procedure. Schoester *et al.* also reported some details concerning the construction of the intramolecular part of the potential for the system. They pointed out that the most accurate model for that part of the potential is the one generated previously by Schmid and Brodbek,[5] whereas a detailed

a)Corresponding author.

description of the force parameters used and some other related information have been presented in the thesis by Schoester.[5] Finally, the major part of that paper discusses only the structural results in conjunction with experimental (x-ray diffraction)[6,7] data. The thermodynamic and dynamical properties of this liquid obtained within the framework of this previous study have not been reported in that or in any other subsequent publication. Therefore, the fundamental question of the reliability of this potential model for liquid DMF and for the other two amides has not yet been definitively answered.

However, before proceeding any further, it is of particular interest to mention here the MC treatments of J. Gao *et al.*,[8–10] devoted to the structural and energetic properties of liquid amides FA, NMA, NMF and DMF at room temperature. In that study, the total potential energy of each liquid consisted of a pairwise additive term (Lennard-Jones plus Coulomb term) and a nonadditive polarization part. The intermolecular potential functions were derived by fitting directly to experimental thermodynamic data for the pure liquids and the polarization energies were optimized to be consistent with the results obtained from combined QM/MM simulations.[9,10] The results obtained from that treatment may be summarized as follows. The calculated heats of vaporization and densities were found to be within 2% and 3% of the experimental results, respectively. The electrostatic and polarization contributions dominate in FA, NMA and NMF, whereas the van der Waals contribution to the potential energy is greater than electrostatic terms for DMF. In the case of DMF, the polarization effects were estimated to be 6% of the total energy which corresponds to about 3%–4% of the system potential energy. Gao *et al.* also found their radial distributions functions to be in agreement with previous results obtained on the basis of the above-mentioned (JS) OPLS model.

Finally, the main conclusion which may be drawn from this MC study is the following. Although one advantage of the PIPF model over OPLS models is its ability to provide valuable information about the polarization effects among the molecules in liquid systems, however, with regards to the properties of liquid DMF, both the OPLS and PIPF approaches are found to predict similar thermodynamic and structural results.

On the other hand, an obvious disadvantage of a PIPF formalism employed in CS studies is that its algorithmic procedure involves usually an iterative self-consistent calculation of the induced dipole moments. The method requires a number of successive iterations in order to achieve the convergence of the induced moments and therefore it is extremely demanding of computer resources. Note also that the implementation of a more precise technique, such as the ''matrix inversion'' method,[11–13] has been found by several workers to be more computationally intensive. The latter method scales as N^3 where N is the number of polarizable sites.

Taking into account all the above considerations, we decided to investigate the physicochemical properties of the pure liquid DMF by performing detailed MD simulations of this molecular liquid over a wide range of temperature. In this MD paper the aim is to demonstrate that the implementation of an accurately optimized intermolecular potential model can also lead to greatly improved predictions regarding not only the energetic and structural properties of the liquid but also the dynamic and transport ones.

The remainder of the paper is organized as follows: The potential models and the simulation details are described in Sec. II. Results are presented and discussed in Sec. III. Finally, our concluding remarks are summarized in Sec. IV.

II. POTENTIAL MODELS AND SIMULATION DETAILS

A. Potential models

As far as we know, previous experimental studies have shown that DMF has no H-bonding possibility in its pure liquid[14,15] phase. Therefore, it may be characterized as a suitable system for the investigation of van der Waals and strong dipolar interactions.

As mentioned in the Introduction, earlier CS studies of liquid DMF were limited to the investigation of the energetic and structural properties by employing mainly the MC method. Other interesting properties for the previously proposed potential models, including their dynamic and transport properties, have not been examined in detail up to date, although two previous MD studies have been devoted to this liquid.[1,4] On the other hand, the employed potential model in a MD study is obliged to reproduce the experimental picture of the simulated liquid as strictly as possible so that artifacts in the analysis of the calculated trajectories can be prevented. This point of view becomes very important when one aims at a systematic computation of various simple and complex properties of the system. However, for MD simulation studies of liquid systems the optimum compromise between the accuracy of the results obtained and the simplicity of the model needs to be found.

At this stage, our first task in a very recent MD treatment of Li^+–Cl^- dissolved in liquid DMF-d7[16] has been to employ an accurate model for the interactions between the solvent DMF molecules. Between OPLS and polarizable models, our attention was focused to the former type since models of that category are computationally simpler. Nevertheless, it should be stressed that a basic argument for this decision has relied on the previous MC predictions of Gao *et al.*[8] with regards to the polarization effects in this liquid.

Thus, in order to fulfill our purpose better, a series of trial NVE and NVT MD simulations was carried out in Ref. 16 with 256 and 500 rigid molecules at 298 and 373 K. In that MD study, the six-site SM OPLS model was used to check to what extent the properties of the DMF liquid depend on the details of the potential. From these preliminary predictions it was possible to draw some conclusions about the reliability of the model in predicting certain properties of the liquid. Note that only some of the results obtained are presented and discussed in Ref. 16. One particularly noticeable area where the SM model had failed was the prediction of the bulk and transport properties. Specifically, we found that in the SM model the mean potential energy is overestimated and too high a pressure is predicted at these state points. Additionally, the self-diffusion coefficients were un-

TABLE I. Parameter values for the available potential models of liquid DMF. PIPF: polarizable intermolecular potential function (Ref. 8); JS: Jorgensen and Swenson (Ref. 2); SM: Schoester *et al.* (Ref. 4); CS1 (Ref. 16); CS2 (this work): Chalaris and Samios.

	PIPF	JS	SM	CS1	CS2
ϵ_{NN}/K_β (K)	78.10	85.58	97.91	84.0	80.0
σ_{NN} (nm)	0.325	0.325	0.3647	0.32	0.32
q_N (e)	−0.560	−0.57	−0.430	−0.57	−0.57
ϵ_{CoCo}/K_β (K)	40.29	52.85	51.96	52.0	50.0
σ_{CoCo} (nm)	0.350	0.375	0.3375	0.37	0.37
q_{Co} (e)	0.450	0.50	0.540	0.50	0.45
ϵ_{MeMe}/K_β (K)	(40.29, 11.08)[a]	85.58	97.91	84.0	80.0
σ_{MeMe} (nm)	(0.350, 0.255)[a]	0.380	0.3807	0.38	0.38
q_{Me} (e)	(0.070, 0.070)[a]	0.285	(0.215, 0.205)[b]	0.285	0.28
ϵ_{OO}/K_β (K)	55.40	105.70	118.56	104.0	100.0
σ_{OO} (nm)	0.295	0.296	0.3405	0.296	0.296
q_O (e)	−0.450	−0.50	−0.510	−0.50	−0.50
ϵ_{HH}/K_β (K)	11.08	⋯	9.76	8.0	8.0
σ_{HH} (nm)	0.255	⋯	0.22	0.22	0.22
q_H (e)	0.00	⋯	−0.020	0.00	0.06
μ (Debye)	4.50	4.45	3.82	4.42	4.41

[a]The first number in parentheses for the PIPF model corresponds to the C atom and the second to the H atom.
[b]The first number in parentheses for the SM model corresponds to the CH_3(cis) and the second to the CH_3(trans).

derestimated in comparison with the experimental values.

The second step in our first treatment towards solving this problem was an attempt to improve the agreement between simulated and experimental thermodynamic results by constructing a reliable OPLS potential model.

As in the case of the SM model, we have decided to construct a model with six interaction sites. The sites were assigned to the positions of all the nuclei of the molecule [H, C_0 O, N, CH_3(tr), CH_3(cis)] except for the hydrogens in the methyl groups. Each CH_3 (*cis* or *trans*) is approximated as one interaction site, located at the methyl carbon.

Concerning the geometry of the molecule in its ground state, x-ray diffraction studies[6,17] have shown that DMF has a nitrogen planar bond geometry, whereas certain gas-phase electron diffraction results indicated a slight nonplanarity of the nitrogen bond configuration.[18] The x-ray results are supported by recent data of *ab initio* calculations at the HF and MP2 levels of theory, as well as functional theory calculations using BLYP and B3LYP functionals,[19] which have revealed that the equilibrium structure of DMF has C_s symmetry with a planar nitrogen bond configuration.

In our treatment a nitrogen planar bond configuration is adopted to mimic the molecular equilibrium geometry of DMF. In order to obtain better agreement with experimental properties considered here, we employed slightly modified bond lengths and angles derived from x-ray studies. They were fixed during our final MD simulations. This modification was realized throughout a series of test simulations which were carried out while the potential parameters $[\sigma_{ij}, \epsilon_{ij}, Q_{ij}]$ were being also readjusted. The parameter optimization procedure employed in our previous study[16] was similar to that widely used in deriving the pairwise OPLS potential parameters for small molecules in condensed phase simulation studies.[20–24] Note that the confirmation of this new set of parameters has been obtained through extensively iterative simulations with trial parameter sets starting from the parameter values of the previously proposed JS and SM models.

Concretely, the initial σ and ϵ values for the hydrogen attached to the C_0 atom were given by the six-site SM model while the hydrogen point charge value was fixed to zero. The new six-site model CS1 was found to be superior to the JS and SM models regarding the bulk properties of the system. However, when compared to some available experimental dynamic properties, it is found that a slight further improvement in the parameters of this model is required to obtain better agreement between simulation and experiment. This is what has been done in the framework of the present MD study, and the set of parameters which best reproduces the thermodynamic and dynamic properties of liquid DMF is our finally proposed potential, referred to hereafter as the CS2 model.

A complete summary of the parameters used for each available model of the present study is given in Table I. The corresponding model geometry of the DMF molecule in its ground state is presented in Table II. As it can be seen from Tables I and II, the parameters of the intermolecular OPLS model, which is taken as a part of the polarizable potential (PIPF) proposed by Gao *et al.*,[8] are also selected for completeness. Note that, in contrast to the other five- and six-site OPLS models, the PIPF model is an all-atom potential.

Let us now discuss the parameter values of the four aforementioned models. To start with, we inspect the molecular geometry parameters assigned to them. It can be clearly seen that, apart from the actual number of interaction sites, the corresponding bond lengths and angles of these

TABLE II. Parameters of the intermolecular geometry of DMF using various potential models for DMF.

	PIPF	JS	SM	CS1, CS2
$r_{NMe(1,2)}$ (nm)	0.1449	0.1449	0.1460	0.1440
r_{CoH} (nm)	0.1090	···	0.1100	0.1123
r_{CoO} (nm)	0.1229	0.1229	0.1230	0.1230
r_{CoN} (nm)	0.1335	0.1335	0.1355	0.1330
$\angle Me_1NMe_2$ (deg)	116.2	121.9	124.0	121.0
$\angle Me_1NCo$ (deg)	121.9	118.3	118.0	120.0
$\angle Me_2NCo$ (deg)	121.9	119.8	118.0	119.0
$\angle NCoH$ (deg)	109.5	···	114.0	114.5
$\angle OCoN$ (deg)	122.9	122.9	123.0	123.0
$\angle HCoO$ (deg)	127.6	···	123.0	122.5

models do differ slightly but not insignificantly from one model to another. Contrary to that, both our proposed models are constructed with exactly the same molecular geometry.

Specifically, for the C=O bond length our model (CS1 or CS2) adopts the same value ($\cong$1.23 Å) as the JS and SM models. With regards to the C_0–N bond length used in our model, however, we see that its value ($\cong$1.330 Å) is almost equal to the x-ray data (1.335 Å). The same value was also imposed by the JS model. In the SM model the C_0–N bond was lengthened by about 0.02 Å relative to the x-ray data. A similar trend can be observed in the case of the N–Me bond length employed in these models. The bond angles involving nitrogen also exhibit small differences from one model to another.

The optimized bond angle $\angle Me_1$–N–Me_2 used in our model is 3° smaller than that in the SM model and 1° smaller than that in JS model. On the other hand, by comparing one by one the bond angles involving the C_0 atom ($\angle HC_0O$,$\angle OC_0N$,$\angle NC_0H$) from the SM and from our model, we can observe that these parameter sets are almost identical. The optimized bond angle $\angle Me_1NC_0$ used in the CS2 model is 2° greater, compared to that in the SM and JS models. Finally the bond angle $\angle Me_1NC_0$ differs by about 1° from one model to another. One can now pay attention to the potential parameter sets assigned to these models and discuss their differences.

As we can see from Table I, the parameter values of the CS1 model differ significantly from those of the SM model. Note that there are only marginal differences between the CS1 parameter values and those of the JS model. This is not the case for our final parameter set values of the CS2 model when compared to the parameter sets corresponding to the JS, SM and CS1 models. Noticeable differences appear between the well-depth parameters mainly for the N–N, Me–Me and O–O interaction sites of these models. Another point of interest is the hydrogen point charge value $q_{H_{Co}}$ assigned in each of the three six-site models. In the SM model, for example, the H_{Co} atom is negatively charged by a point charge of -0.02 e, whereas in model CS2 the same interaction site is positively charged by a point charge of 0.06 e. The fractional charge distribution used in the SM model is determined by using a previously reported charge distribution for DMF determined on the basis of semiempirical CNDO calculations.[25] Also, the pattern of charge distribution in our CS1 model, with $q_{H_{Co}}=0$ e, comes out to be the same with that employed in the five-site JS model for DMF which is similar to the Hagler–Lifson[26] potential for amides.

To the best of our knowledge, a fractional charge distribution for DMF from *ab initio* calculations has not yet been published, although such theoretical treatments have been reported.[19,27,28] In contrast, fractional charge distribution for FA is already available from *ab initio* calculations[29] of J. Richardi. In that study, the evaluation of the charge distribution in FA shows that the $q_{H_{Co}}$ is positive (0.03 e). The above result has been taken into account in our attempt to reevaluate the potential parameters for DMF. This was justified because of the similarities between these two molecular systems. The charge $q_{H_{Co}}$ in DMF for our CS2 model is set more positive by 0.03e. The point charge distributions used for the DMF models yield effective dipole moments generally (i.e., except in the SM model) higher than the gas phase dipole moment. This fact is in agreement with the consideration that point charge distributions need to yield dipole moments greater than gas-phase values in potential models designed for liquid simulations. As we can see from Table I, in the case of the CS2 model the corresponding charge distribution yields a dipole moment about 12.5% higher than the gas-phase value.

Finally, we have found that the combination of the above charge distribution with appropriate modification of the LJ parameters and molecular geometry led us to the construction of a new more accurate six-site potential for the DMF liquid.

B. Simulation details

In the present study, the liquid phase of pure DMF at two state points corresponding to 298 and 373 K was extensively simulated using the NVE and NPT-MD methods. For each potential model we carried out simulations with 256 and 500 molecules in the central simulation box with periodic boundary conditions. Also, the well-known Ewald summation method is employed to account for the corrections of the long range electrostatic interactions. In all cases, a spherical cutoff with half the box length as the cutoff distance was used to truncate the short range interactions. Molecular orientations have been treated with the quaternion formalism whereas the translational and rotational equations of motion are integrated using leap-frog algorithms. Initial configurations were based either on the FCC lattice with densities corresponding to the experimental state points or on previous MD runs carried out under similar conditions. In all cases, the employed integration time step was 3 fs.

Each model liquid was simulated for a relative long time interval of about 1 ns. From this period, the first 200 ps were regarded as the time interval to reach equilibrium and the rest to calculate the properties of the system.

The results obtained for the four models are presented and discussed in the following sections.

TABLE III. Thermodynamic results for liquid DMF at 298 and 373 K from the present and previous studies by using various potential models. Depicted are the number of the molecules used, N; the temperature, T (K); the molar volume, V_m (cm^3); the average potential energy, U_P ($KJ\,mol^{-1}$); the pressure, P (bar), as well the mean square force, $\langle F^2\rangle$ ($10^{-18}\,N^2$); and torque, $\langle T^2\rangle$ [$10^{-20}\,(Nm)^2$], acting on each molecule of the system.

	$T=298$ K							
	JS-MC[a]	JS-MD[c]	JS-MD	SM-MD	CS1	CS2		EXP
	NPT	NVE	NVE	NVE	NVE	NPT	NVE	⋯
N	128 256	64	256	256	256	500	500	⋯
T	298.0	294.2	297.8	297.7	297.3	298.0	296.9	298.0
V_m	77.1044	77.431	77.431	77.431	77.431	77.761	77.431	77.431
$-U_{\text{pot}}$	45.42–44.75	44.1	43.74	47.94	44.16	44.32	44.38	44.4
P	1	⋯	138.3±189.3	1224.4±197.2	128.04±190.28	1	46.8±200.2	1
$\langle F^2\rangle$	⋯	⋯	0.259	0.298	0.257		0.257	⋯
$\langle T^2\rangle$	⋯	⋯	0.426	0.516	0.439		0.438	⋯
	$T=373$ K							
	JS-MC[b]		JS-MD	SM-MD			CS2	EXP
	NPT		NVE	NVE		NPT	NVE	⋯
N	128		256	256		256	256	⋯
T	373.0		381.2	367.0		373.0	372.3	373.0
V_m	83.06		83.728	83.728		83.41	83.728	83.728
$-U_{\text{pot}}$	40.81		39.195	43.316		40.61	40.38	40.43
P	1		118.71±201.5	462.6±212.5		1	−71.85±211.1	1
$\langle F^2\rangle$	⋯	⋯	0.282	0.328	⋯		0.279	⋯
$\langle T^2\rangle$	⋯	⋯	0.472	0.566	⋯		0.478	⋯

[a,b,c]From Refs. 3, 2, and 1, respectively. The estimated errors were maximal: ±3 K for T, ±1% for U and less than 1% for V_m.

III. RESULTS AND DISCUSSION

A. Thermodynamics

The mean potential energy, U, the pressure, P, of liquid DMF, and the mean squared (ms) values of the force, $\langle F^2\rangle$, and torque, $\langle T^2\rangle$, which act on each molecule due to its surrounding molecules, have been calculated using the four OPLS models and they are summarized in Table III together with the corresponding experimental data at 298 and 373 K. In Table III some results obtained in previous CS of the DMF liquid are also depicted for comparison. The experimental mean potential energy of the liquid U_p^{Exp} is obtained from the available heat of vaporization via the well known Eq. (1):

$$\Delta H_{\text{Vap}}^{\text{Exp}} = U_{\text{intra}}(g) - [U_p^{\text{Exp}} + U_{\text{intra}}(l)] + RT, \tag{1}$$

having assumed that the intramolecular rotational energy for the gas, $U_{\text{intra}}(g)$, is equal to that for the liquid, $U_{\text{intra}}(l)$, at the state points under investigation. This assumption is based on the fact that previous model calculations have shown no change in $U_{\text{intra}}(g)$ upon passing from the gas state to the liquid (see Table IV in Ref. 2).

A closer inspection of the results presented in Table III indicates clearly the strength or the weakness of each proposed OPLS model in describing successfully the thermodynamics of this liquid. As we can see, comparisons among these models reveal the following specific features: Concerning the mean potential energy U_p at 298 and 373 K, we clearly see that the six-site SM model overestimates this property by about 3.54 $KJmol^{-1}$ (≅8%) at 298 K and by about 2.9 $KJmol^{-1}$ (≅7%) at 373 K. Moreover, we found this model to give a pressure of 1200±210 bar at 298 K and 460±250 bar at 373 K, which is unreasonable compared with experimental results.

In the case of the five-site JS model, the picture emerging from our NVE-MD data for the potential energy is in agreement with previous NPT and NVT-MC studies[2,3] where long range electrostatic interactions were also incorporated in the form of a reaction field ($\epsilon_{\text{rf}}=1$ or ∞). The MC studies at 298 K with 128 and 256 molecules, for instance, yield potential energy values in the range of 44.75–45.42 $KJmol^{-1}$, whereas our NVE-MD simulation with 256 molecules yields a somewhat smaller value of 43.74 $KJmol^{-1}$. We do conclude, however, that all the CS predictions for the potential energy with the model JS are quite close to the experimental value of 44.4 $KJmol^{-1}$. A similar conclusion may be drawn from this property in the case of 373 K.

Finally, by inspecting the pressure obtained from the present NVE-MD simulation studies, we see that the JS model produces better results than the six-site SM model when compared to the experiment. As it becomes apparent from the NPT-MC simulation, the JS model underestimates the molar volume V_m of the liquid by about 0.330 and 0.668 $cm^3\,mol^{-1}$ at 298 and 373 K, respectively. Therefore, the JS model overestimates the density of the liquid at both temperatures. Note that at 373 K this result deviates from the experimental data by about 3%.

As we can see from Table III, the results from the model CS2 are considerably better than those obtained using the two previous models JS and SM and with the CS1 model, which nevertheless provides a better level of accuracy when compared to the former two models. As far as the mean potential energy is concerned, the CS2 model can reproduce

TABLE IV. The electrostatic and LJ contributions to the total average potential energy of liquid DMF calculated in the frame work of this study (potential models JS, SM, CS2) and from previous computer simulation studies (PIPF) and theoretical investigations of this liquid (MOZ-PC, MOZ-a1). Numbers in parentheses give the relative contributions in percent.

	$-U_{LJ}$ (KJ mol^{-1})	$-U_{EL}$ (KJ mol^{-1})	$-U_{pot}$ (KJ mol^{-1})
JS 298 K	29.10 (66.53)	14.64 (33.57)	43.74
373 K	26.07 (66.52)	13.13 (33.5)	39.19
SM 298 K	38.1 (79.50)	9.83 (20.50)	47.9
373 K	34.9 (79.86)	8.82 (20.18)	43.7
CS2 298 K	28.2 (63.54)	16.18 (36.46)	44.38
373 K	25.46 (63.02)	14.94 (36.98)	40.4
PIPF[a] 373 K	22.9 (56.13)	17.9 (43.87)	40.8
MOZ-PC[b] 298 K	26.1 (68.50)	12.0 (31.50)	38.1
MOZ-a1[b] 298 K	26.0 (64.68)	14.2 (35.32)	40.2

[a]Reference 10.
[b]Reference 29.

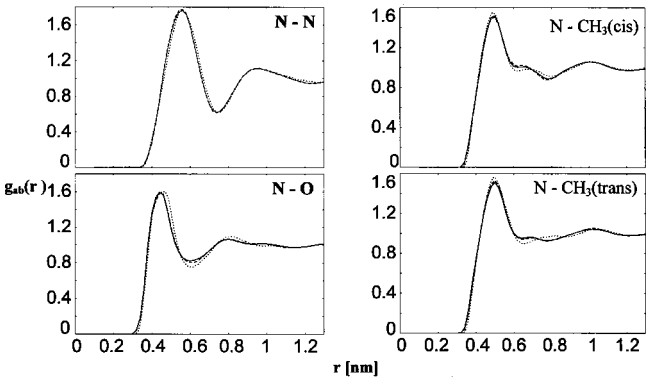

FIG. 1. Site–site pair distribution functions of liquid DMF at 298 K for the three different potential models (———CS2; – – –JS; ---SM) from this MD study.

the experimental results of the system quite well, within less than 1% at both temperatures. Moreover, with regards to the simulated pressure and density, the CS2 model can reproduce these thermodynamic quantities better than the previous models, having taken under consideration the fact that these properties can be calculated with low accuracy in general. Therefore, our new optimized model proved to be clearly superior than the previous ones, covering almost the complete temperature range of the liquid state at atmospheric pressure.

Additionally, we have investigated the relative importance of the electrostatic and dispersion interactions in the mean potential energy of the liquid. To achieve this we have calculated the separable contributions which arise due to the LJ and Coulombic terms U_{LJ} and U_{EL}, respectively. Our CS results obtained for the various investigated potential models at both temperatures are presented in Table IV together with some theoretical[29] and MC data[8] which were borrowed from the literature.

Note that the theoretical data in this table were obtained within the framework of the hypernetted chain (HNC) approximation of the molecular Ornstein–Zernike (MOZ) theory at 298 K. In that treatment,[29] the employed unpolarizable model assumes that a molecule carries only partial charges on its interaction sites (MOZ-PC). This assumption was based on the charge distribution used in the PIPF potential model of Gao *et al.*[10] For the polarizable model used (MOZ-a1), an additional induced dipole is placed at the molecular center of mass. In that case, the effects of the molecular polarizability were considered along the lines of a self-consistent mean-field (SCMF) theory.

By inspecting the simulated and theoretical results presented in Table IV, it is clearly seen that in all cases both energetic terms contribute significantly to the intermolecular potential energy. It is also seen that the LJ part is the major contribution compared to that of the electrostatic part. Specifically, in the cases of the JS-MD, CS2-MD, MOZ-PC and MOZ-a1 model calculations, the ratio value U_{LJ}/U_{EL} is approximately 2, whereas for the SM-MD and PIPF-MC models this ratio is about 4 and 1.3, respectively. One also observes that the LJ parts of the potential energy U_{LJ} obtained from each of the four model CS_s are different from each other at the same temperature. In contrast to these CS predictions, the two theoretical approaches yield strictly comparable U_{LJ} results. This occurs due to the fact that the LJ contribution is almost independent of the polarizability when its effect is taken into account. Note that these two theoretical predictions for the LJ part are certainly smaller in comparison to the corresponding CS values at 298 K. Furthermore, the internal electrostatic energy U_{EL} changes significantly when the polarizability is taken into account (MOZ-a1 model), something which is expected. Also, the U_{EL} values from all of the six model calculations are found to be different from each other at the same state point of investigation. Finally, it is found that the calculated total internal energy of the liquid at 298 K obtained on the basis of the two theoretical models MOZ-PC and MOZ-a1 is underestimated by about 6 and 4 KJ mol^{-1}, respectively. The author in Ref. 29 suspects that this is presumably due to the deficiency of the SCMF approximation when applied to polar molecules with quite large polarizabilities.

B. Liquid structure

Let us now investigate how the simulated intermolecular structure of liquid DMF varies with the potential models employed in the present MD studies.

As in previous CS studies, the intermolecular structure of the liquid has been investigated in terms of the various site-site pair radial distribution functions (rPDFs), $G_{ab}(r)$. This function represents the probability of finding an atom b of the molecule j at a distance r from an atom a of the molecule i. The various rPDFs have been evaluated for correlation distances up to about 12 Å with a resolution of 0.1 Å for both of the state points of interest. The present MD results for these distribution functions obtained at 298 K and for the models JS, SM and CS2 are shown in Figs. 1–3. Figure 4 shows how the shape of some of these rPDFs [$G_{N-N}(r)$, $G_{O-O}(r)$ and $G_{C_0-C_0}(r)$], obtained with model CS2, varies with temperature at normal pressure.

The inspection of the curves which appear in Figs. 1–3 confirms that the qualitative trends observed in the rPDFs for the previous two models, i.e., JS and SM, are also observed

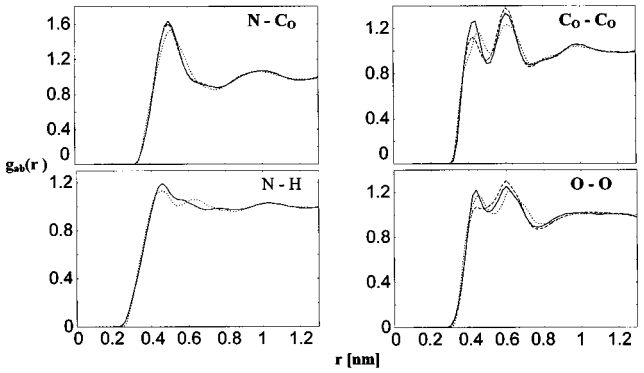

FIG. 2. The same description as in Fig. 1.

in the corresponding functions obtained using our new model, CS2. However, some differences can be observed between the structural directing effects produced by these models at the same thermodynamic conditions. We recall that the group CH_3(cis) is the methyl group next to the oxygen atom. Thus, regarding the rPDFs separately, the most pronounced structural differences appear in the behavior of the functions displayed in Fig. 3 [CH_3(cis)–O, CH_3(trans)–O, C_0–O, H–O] and in Fig. 2 (C_0–C_0, N–H, O–O). On the contrary, each function of the type $G_{N-X}(r)$ [X=N, O, CH_3(cis), CH_3(trans)], presented in Fig. 1, and the function $G_{N-C_0}(r)$ presented in Fig. 2, shows quite similar behavior in going from one model to another. This is apparent from the positions and heights of the characteristic extrema of the depicted correlations. Note that the positions and heights of the first maximum and minimum, as well as the calculated coordination numbers, n_{ab} at 298 K, of some of these functions are collected and compared in Table V.

In what follows we will first discuss in detail some of the present MD rPDFs in conjunction with findings from prior CS studies of the DMF liquid. Thus, concerning the N–N distribution seen in Fig. 1, which, in a first approximation, can be considered as the center of mass (COM-COM) rPDF of the system, we observe a single broad first peak followed by a distinct second maximum. In all models, the first peak is located at relatively large distance (5.6 Å) whereas the height varies only from 1.76 (SM and CS2 models) to 1.77 (JS model). Integration of this distribution up to the first peak

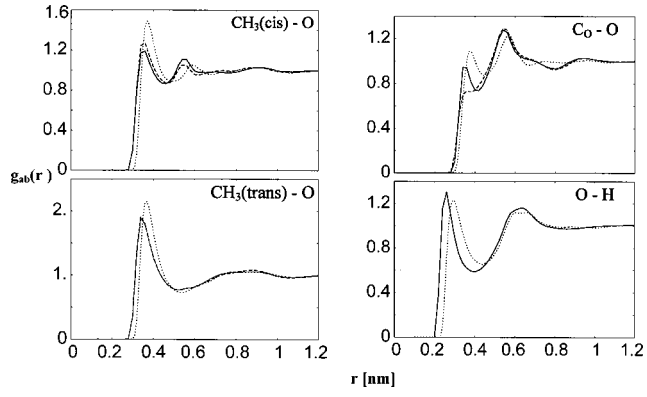

FIG. 3. The same description as in Fig. 1.

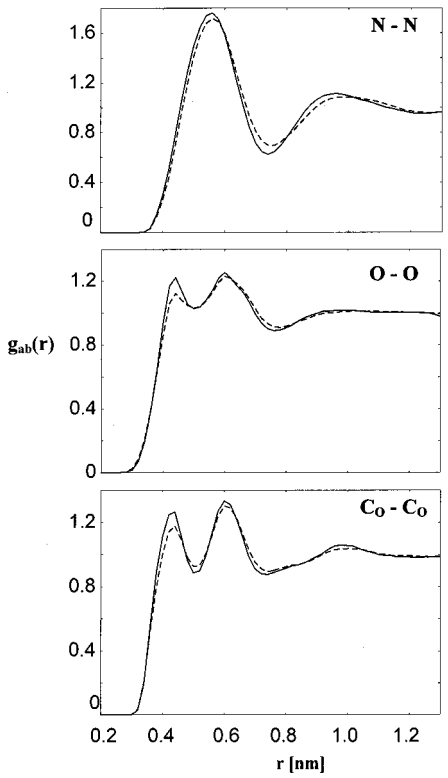

FIG. 4. Temperature dependence of the site–site pair distribution functions (N–N, O–O, C_0–C_0) of liquid DMF for the CS2 potential model from this MD study (———298 K; – – –373 K).

yields 4.4 neighbors for the SM model, and 5.3 for the JS and CS2 models. One should add that for all models, the coordination number calculated up to the first minimum is found to be about 13. By comparing all the present MD results for the N–N distribution with those from the previous MC and MD studies,[1,3,4] we have found out that there is good agreement among all of them apart from those obtained from the PIPF-MC simulation of Gao *et al.*[10] In the latter case, the short range part of the N–N function consists of two overlapping peaks, in contrast to the rest of the models for which the short range part of the function is single peaked.

Eventually, from Fig. 4 it is obvious that the shape of the N–N distribution does not change considerably when the temperature and consequently the density of the liquid is varied at normal pressure. This result indicates strong similarities in the constructed intermolecular structure of DMF upon passing from room to a higher temperature.

Some other distribution functions such as the CH_3(cis)–O, CH_3(trans)–O, O–O and H–O, which correspond to the peripheral interaction sites of the molecules, exhibit pronounced first peaks at relatively shorter distances in comparison to the other site-site distributions. Moreover, as it can be seen from Figs. 1–3 and Table V, the first peak of the CH_3(trans)–O function appears to be more intense than the first peaks of the three other aforementioned functions. The overall behavior of each of the four rPDFs is found to be quite similar in all models used in the present MD study, as well as in good accordance with the results

TABLE V. Positions and amplitudes of the first maximum and minimum [r (Å):$G(r)$] as well the calculated coordination numbers ($n_{\alpha\beta}$) of the various site–site pair distribution functions of liquid DMF for the potential models JS and SM and for the present model CS2 obtained in this study.

	JS		SM		CS2	
	First maximum r (Å):$G(r)$ $n_{\alpha\beta}$	First minimum r (Å):$G(r)$ $n_{\alpha\beta}$	First maximum r (Å):$G(r)$ $n_{\alpha\beta}$	First minimum r (Å):$G(r)$ $n_{\alpha\beta}$	First maximum r (Å):$G(r)$ $n_{\alpha\beta}$	First minimum r (Å):$G(r)$ $n_{\alpha\beta}$
N···O	4.40:1.584	6.0-6.2:0.802	4.60:1.608	6.10:0.749	4.40:1.592	6.0:0.820
	4.0	13.18-14.39	4.82	13.56	4.03	13.17
Me1···O	3.60:1.268	4.60:0.873	3.70:1.492	4.90-5.0:0.893	3.60:1.189	4.6:0.867
	1.61	4.97	1.40	6.54-6.9	1.53	4.76
Me2···O	3.40:1.908	5.2:0.767	3.70:2.148	5.3-5.4:0.725	3.40:1.885	5.2:0.768
	1.52	8.66	2.11	9.1-9.4	1.53	8.64
C_0···O	3.60:0.735	4.20:0.926	3.80:1.09	4.50:0.87	3.40:0.945	4.20:0.74
	0.96	2.90	1.35	3.61	0.68	2.59
O···H	···	···	2.90:1.23	4.51:0.65	2.60:1.304	4.0:0.586
			0.67	3.95	1.944	2.956
N···N	5.60:1.774	7.40:0.615	5.50:1.76	7.50:0.610	5.60:1.761	7.40:0.623
	5.31	13.18	4.39	13.42	5.30	13.17
N···C_0	5.0:1.604	7.60:0.875	5.10:1.527	7.40:0.852	5.0:1.633	7.6:0.878
	6.36	27.76	6.41	25.35	6.35	27.77
C_0···C_0	4.2:1.123	5.0:0.912	4.50:1.170	5.20:0.970	4.40:1.265	5.0:0.887
	1.18	2.89	1.68	3.42	1.69	3.03

found in all previous CS studies of the liquid. This behavior can be explained in terms of the strong dipolar interactions and steric effects among neigboring molecules. Thus, our JS-MD results support the suggestion made in the framework of previous CS studies[1,2] where the JS model was used, that the DMF molecules tend to form some preferential local order at intermolecular distances of up to about 5.5 Å. This suggestion is also in agreement with NMR studies.[15] Nevertheless, it is in contrast with conclusions obtained from a previous x-ray diffraction study[6] of DMF at room temperature.

Specifically, the authors pointed out in Refs. 1 and 2 that the nearest molecular ordering in DMF can be interpreted with a stacked parallel-plate arrangement with dipoles aligned in opposite directions. This was based on their rPDFs and some specific[30] orientational correlation functions. Furthermore, the authors concluded in Ref. 1 that the next neighbor molecules, i.e., those beyond 5.5 Å, are oriented so that both the molecular planes are perpendicular to each other and to the line joining their centers of mass. This is the well-known cross (+) shaped configuration.

In order to check for the correctness of the local structure, proposed by these authors (Ref. 1) on the grounds of relatively short phase space MD trajectories, we applied their procedure here using sufficiently long trajectories. From such an analysis of our MD-JS results, the predominant nearest local order of the molecules was found to be close to the previous predictions.

On the other hand, the question to what extent the differences in the potential models can influence the calculated structural properties of liquid DMF has also been a matter of investigation in the present study. Thus, by comparing the rPDFs from the model with the five-site interpretation with those from the six-site models (SM or CS2), some systematic differences can be observed between them; specifically at short correlation distances of up to about 6 Å. Therefore, we should be careful in concluding definitively about the most probable local order amongst the molecules in DMF. For example, we may observe from Fig. 3 that the most intense CH_3(trans)–O functions, from the JS and CS2 potentials, are very similar. However, the same function from the SM model differs significantly from the former two models. Thus, the first peak is higher (2.148) with the SM model and occurs at longer distances (3.7 Å) in comparison with the other models.

The CH_3(cis)–O distributions are also somewhat differently shaped from one model to another. Differences between them are visible not only in the formation of the first peaks, but also in the formation of the second ones.

The situation becomes more complicated in the case of $G_{C_0-O}(r)$, seen in Fig. 3. The results of the model JS exhibit a plateau between 3.6–3.9 Å followed by a broad peak located at about 5.1 Å. This behavior is somewhat different compared with the corresponding MC results for the JS model reported in Ref. 2. Furthermore, from the present results it is clearly seen that the $G_{C_0-O}(r)$, obtained from the SM and CS2 models, is more structured compared to that from the JS model. This may be justified by the existence of a twin peak on the C_0–O functions from the six-site models, SM and CS2, which is located at short distances.

Concerning now the O–O rPDFs seen in Fig. 2, we observe that these correlations exhibit qualitatively a similar behavior compared to the C_0–O functions from one model to another.

Eventually, it should be noted that the structural results reported here include the behavior of the O–H distribution for the first time from a six-site (SM and CS2) model. From Fig. 3, it is clearly seen that the results for the O–H function from both models are qualitatively similar. However, the first peak is somewhat higher with the CS2 and occurs at a shorter distance than that with SM. In addition, it appears at

the shortest distance (2.6 Å) when compared to any other peripheral site-site distributions. It cannot escape our attention that, although the H atom is very close to the C_0, the C_0–O and H–O distributions are totally differently shaped.

The above results provide additional insights regarding the microscopical structure in liquid DMF. They can be a sign of the existence of some other molecular orientational ordering, which may be less probable than the most favorable one, for which the planes of two neighbor molecules are nearly parallel with the dipoles of the opposite direction. This is due to the fact that the very short O..H contacts cannot be explained geometrically in terms of the local order discussed above. In a such local order, the O–H contact distance is sufficiently greater than 2.6 Å. In addition, we have from Table V that the first peak in O–H appears at about a 3 Å lower r value than the first peak distance in N–N, which defines approximately the nearest neighbors.

We recall here that the authors in Ref. 1 also proposed another less probable molecular arrangement: that of the cross (+) type for COM-COM separations beyond about 5.5 Å. However, even in this case our MD results for the O–H distribution cannot be explained by assuming this type of dimmer structure. It is interesting to notice here that, if we assume that the two molecular planes are shifted from the + shaped arrangement to one of the X type, it is then possible to explain geometrically the O–H contacts at approximately 2.6 Å as well as some of the characteristics of other distributions. Furthermore, another possible molecular dimmer arrangement, which can be deduced from the above O–H and C_0–O results, is one in which the two molecules are arranged into a tail-to-tail type for nearly coplanar configurations.

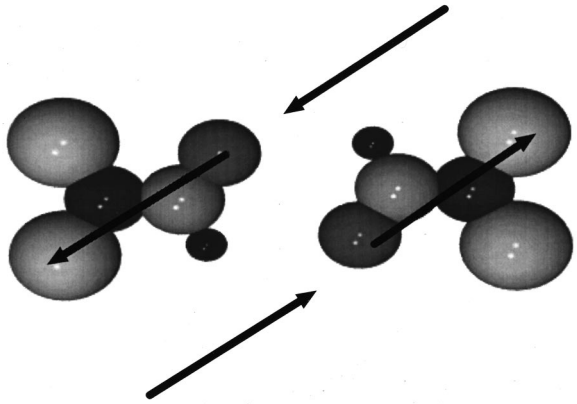

Such an orientational ordering could also be anticipated for reasons of electrostatics. By assuming, for example, a linear chain of dipoles arranged into a head-to-tail direction, one could expect that the dipoles from the neighbor chains are oriented in opposite directions. Let us, for instance, consider a two-dimensional scheme in which two nearest DMF molecules belong in neighbor chain molecules. These two molecules form a tail-to-tail dimmer configuration in which the H atom of the first molecule is in contact with the O atom of the second one and vice versa. However, with regards to the intermolecular energy minimum, such a type of structuring in the liquid cannot be energetically stable enough. Note that in the above configuration the N–N separation is beyond 6.3 Å. Therefore, one could expect that the interactions of these two molecules with neighboring molecules lead to somewhat different dimmer order in comparison to the latter idealized one.

By taking all the above considerations into account, we may conclude that the present MD study of liquid DMF, with the six-site CS2 model, yields comparable structural results with previously proposed potential models. The somewhat contrasting behavior of some peripheral site-site rPDFs for the CS2 model with respect to the JS and SM models indicates the existence of some enhanced molecular order not only for the nearest neighbor molecules but also for the next nearest ones.

Finally, the reliability of all the structural results obtained with these models should be judged from their comparison with suitable real experimental data. Neutron diffraction (ND) experiments with isotope substitution are suitable in principle to predict structural data on molecular liquids, by determining the various atom-atom distribution functions. Since, however, ND studies have not been performed on liquid DMF, a definitive solution to the problem of the microscopical intermolecular structure in the fluid cannot be given at the present time.

C. Transport properties

As mentioned in the Introduction, the evaluation of the transport properties of the investigated models is also included in the framework of the present MD study. Specifically, the investigation of the dynamical and transport properties of the system allowed us to explore the accuracy of the employed potential models from another point of view and to provide additional information regarding the behavior of the DMF liquid. Moreover, this is the first time the abovementioned properties of the system based on the available potential models have been extensively studied using MD simulation techniques.

In CS studies the transport coefficients of a fluid can be obtained using the Green–Kubo integrals of the correlation functions of the corresponding microscopic fluxes, i.e., the sums over specific elements of the tensors.

In the present study, the self-diffusion coefficients were calculated from the mean-square displacements (MSD) of the molecules, using the well-known Einstein relation:

$$6D = \lim_{t\to\infty} \frac{1}{t} \langle [\Delta r(t)]^2 \rangle. \tag{2}$$

In the calculation of the MSD of each molecule in the sample, the molecule positions are not subjected to periodic boundary condition shifts and can take values outside the simulation box. In order to obtain reliable results, we have used very long MSD plots of about 350 ps, from which only the last 150 ps were taken into account for the estimation of the coefficients.

The shear viscosity was obtained from the correlation function of any of the off-diagonal elements of the symmetric part of the pressure tensor, following the well-known Green–Kubo relation

$$n = \frac{V}{k_\beta T} \int_0^\infty \langle J_p^{xy}(t) \cdot J_p^{xy}(0) \rangle dt, \tag{3}$$

TABLE VI. The calculated transport properties (single diffusion D and shear viscosity n_s) of liquid DMF at 298 and 373 K from this MD study for the potential models JS, SM and CS2. For comparison the corresponding experimental values at 298 K have also been selected.

	298 K		373 K	
Models	D (10^{-9} m^{2}s^{-1})	n_s (cp)	D (10^{-9} m^{2}s^{-1})	n_s (cp)
JS	1.40	0.55	3.60	0.29
SM	0.80	1.01	2.29	0.38
CS2	1.25	0.72	3.44	0.28
EXP	1.63[a]	0.80[a]	⋯	⋯

[a]Reference 33.

where V is the volume and T is the temperature of the system. J_p^{xy} indicates the xy element of the pressure tensor $\mathbf{J}_p$, which, in the case of a system of N molecules, each molecule consisting of n atomic centers, can be expressed as follows:[31]

$$V\vec{J}_p=\frac{1}{m}\sum_{\alpha=1}^{N}\vec{p}_\alpha\vec{p}_\alpha-\frac{1}{2}\sum_{\alpha\neq\beta}^{N}\sum\sum_{i,j}^{n}\vec{R}_{\alpha\beta}\nabla U(r_{\alpha\beta}^{ij}). \quad (4)$$

In Eq. (4) α, β denote the molecules and i, j the atomic centers. R refers to molecule and r to the atom centers. $\vec{R}_{\alpha\beta}$, $r_{\alpha\beta}^{ij}$ denote the difference of two center of mass position vectors of molecules α and β, and the separation of the atomic centers, respectively. U denotes the pair potential function between the atomic interaction sites and $\vec{p}_\alpha$ the momentum of the α molecule.

In the case of molecular systems, the off-diagonal elements of the tensors are generally not equal. So, one must take care to symmetrize the tensor $\mathbf{J}_p$. To overcome this problem the shear viscosity must be evaluated by using a symmetrized form of the tensor elements.[32] We notice that the symmetrization procedure is not needed in the kinetic part of the tensor. In each case, the shear viscosity was calculated using time trajectory of about 0.8 ns, during which the off-diagonal elements of the pressure tensor were saved for every time step.

Both the diffusion and the shear viscosity coefficient at 298 and 373 K, obtained for the JS, SM and CS2 models, are presented in Table VI together with available NMR results at 298 K reported by M. Holz *et al.* (see Tables II, III and IV in Ref. 33). The comparison of the self-diffusion coefficients suggests that the JS and CS2 models provide the best agreement between calculated and experimental data. In addition, the SM model underestimates the mobility of DMF molecules in the liquid. In the case of the shear viscosity, it is clearly seen that the CS2 model predicts the best results in comparison to the rest of the models. Finally, we observe that these two calculated transport properties show the correct temperature dependence.

D. Dynamical properties

For the study of the dynamical properties of the liquid DMF, it is convenient to calculate and analyze the appropriate time correlation functions (CFs) of some dynamical variables of the system.

TABLE VII. Calculated correlation times τ_c (ps) of liquid DMF at 298 and 373 K for the employed potential models JS, SM and CS2 from this MD study. Some experimental data have been also selected for comparison. Depicted are: the linear velocity, τ_U; the angular momentum, τ_J; and the times τ_1^c, τ_1^b, τ_2^c, τ_2^b from the first and second order Legendre polynomials ACFs (c, b denotes the two principal axes of the molecule).

	298 K					
	τ_U	τ_J	τ_1^c	τ_1^b	τ_2^c	τ_2^b
JS	0.046	0.037	5.42	4.41	2.0	1.78
SM	0.030	0.025	9.57	8.30	3.51	3.59
CS2	0.044	0.033	6.63	5.50	2.24	2.01
EXP	⋯	⋯				2.4[a]
	373 K					
JS	0.081	0.060	2.64	2.23	0.94	0.88
SM	0.061	0.048	3.72	3.27	1.34	1.32
CS2	0.083	0.058	3.21	2.70	1.14	1.003
EXP	⋯	⋯	⋯		⋯	

[a]Reference 38.

A simple way of describing the single translational motion of the molecules in the fluid is by means of the COM linear velocity autocorrelation function (VACF) $C_v(t)$ defined by the following expression:

$$C_v(t)=\frac{\langle\vec{v}(0)\cdot\vec{v}(t)\rangle}{\langle\vec{v}(0)^2\rangle}. \quad (5)$$

These ACFs have been calculated at both temperatures, and the corresponding correlation times τ_v for the employed potential models JS, SM and CS2 are selected in Table VII. The times τ_v have been obtained by integrating the VACFs up to 2 ps. In Fig. 5(a) we show the VACF of liquid DMF obtained with the CS2 model at 298 and 373 K.

The $C_v(t)$ curves displayed in Fig. 5(a) show the following qualitative behavior. The $C_v(t)$ at 298 K goes rapidly to zero in less than 0.15 ps. Afterwards it shows a shallow negative minimum (anticorrelation region) and then converges to zero after $\cong$1 ps. We may also observe that the anticorrelation region of the above curve exhibits a small double minimum structure. In order to illustrate this feature, it is common to split the VACF into three components along the x-, y- and z-directions. Yashonath and Rao[1] reported the results of a similar analysis. They pointed out that the overall molecular translational motion is anisotropic at room temperature.

The temperature dependence of the translational motion of the molecules is also indicated in Fig. 5(a). The depth of the negative minimum of the $C_v(t)$ decreases as the temperature increases, denoting a relative enhancement of the diffusive character of the molecular motion.

Let $\hat{u}_c$ and $\hat{u}_b$ be the unit vectors along the principal rotational axes c and b of the molecule. The single rotational dynamics of the system have been studied by means of the angular momentum ACF, $C_J(t)$, and the first and second order Legendre reorientational ACFs, $C_L(t)$, of these two unit vectors, respectively:

$$C_L^x(t)=\langle P_L(\hat{u}_x(0)\cdot\hat{u}_x(t))\rangle, \quad x=c,b;L=1,2. \quad (6)$$

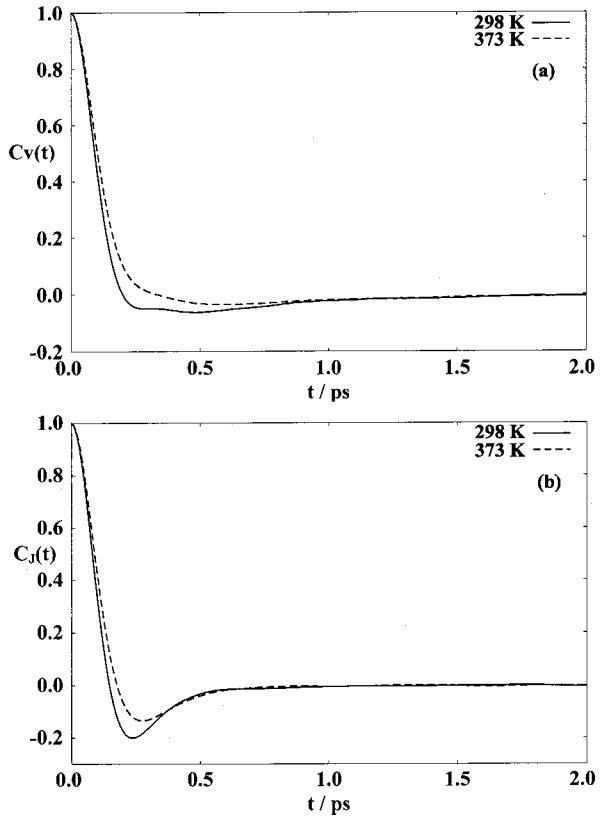

FIG. 5. Time autocorrelation functions of the linear velocity $C_v(t)$ (a) and of the angular momentum $C_J(t)$ (b) of liquid DMF for the CS2 potential model at 298 K (———) and (– – –) 373 K.

Legendre correlations for the unit vector $\hat{u}_a$ of the third principal rotational axis *a* have not been obtained. In the case of the model CS2, the moment of inertia for the axis *a* ($I_a = 0.480\,63\ \text{amu}\cdot\text{nm}^2$) is smaller by a factor of 2 and 3 in comparison to that of the axis *b* ($I_b = 1.083\,65\ \text{amu}\cdot\text{nm}^2$) and that of *c* ($I_c = 1.564\,28\ \text{amu}\cdot\text{nm}^2$), respectively. This explains why we have been dealing mainly with axes *b* and *c*. In the following schematic representation, the axis *c* is perpendicular to the *ab* plane and mc denotes the mass center of the DMF molecule.

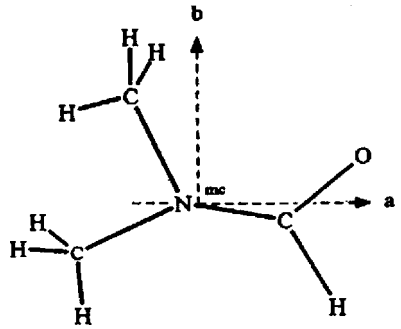

All the above ACFs have been evaluated at both temperatures and their estimated correlation times are depicted in Table VII. The results for the $C_J(t)$ ACFs with the CS2 potential are shown in Fig. 5(b). The correlation times τ_j have been obtained by integrating the angular momentum ACFs up to 2 ps. From Fig. 5(b) one notices that the angular momentum ACFs display a different behavior in comparison to that of the linear velocity ACFs. We thus observe a well-formed deep and single minimum at negative values which are located at $\cong 0.24$–0.27 ps. The negative portions of these ACFs decay very fast to zero at $t \cong 0.65$ ps and display a temperature dependence. It is well known that, in molecular liquids with high torques, the angular momentum ACFs exhibit nonexponential behavior,[34] often showing negative parts. This behavior leads to describing the motion in terms of a librational type motion. The angular ACFs of DMF display an analogy to the ACFs discussed above. As we can see below, no indication of strong librational motion of the DMF molecules is observed which would give rise to a shoulder in the Legendre ACFs, $C_L(t)$.

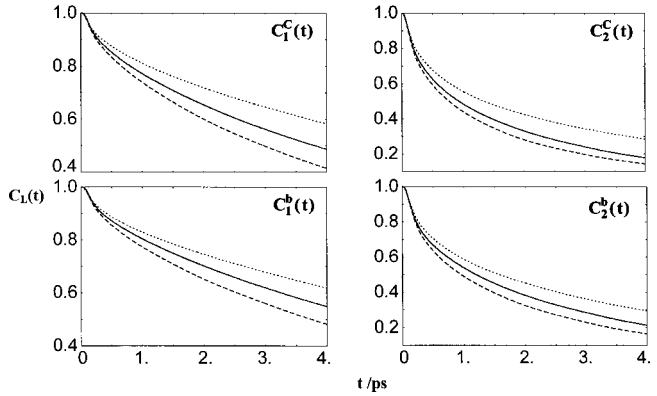

FIG. 6. Time autocorrelation functions of the first $C_1^c(t)$, $C_1^b(t)$ and second $C_2^c(t)$, $C_2^b(t)$ order Legendre polynomials of liquid DMF at 298 K and for the three different potential models used: (———CS2); (– – –JS); and (---SM).

The results for the Legendre ACFs, namely $C_1^c(t)$, $C_1^b(t)$, $C_2^c(t)$ and $C_2^b(t)$ at 298 K and for the three models (JS, SM and CS2), are shown in Fig. 6. The single molecule reorientational correlation times $\tau_L^x (L=1,2; x=b,c)$ can be estimated by integrating the ACFs or by fitting these functions using an exponential function of the form:

$$C_L^x(t) = A \cdot \exp\left[-\frac{t}{\tau_L^X} \right]. \tag{7}$$

As we can see from Fig. 6, these ACFs converge very slowly to zero. Therefore, in order to calculate the corresponding correlation time, we have employed a combined method. According to this method, we used explicit numerical integration up to 2 ps, and fitted the rest of each ACF to Eq. (7). We obtained analytically the integral for the rest of the function from the fit.

By inspecting the predicted correlation times, τ_L^x, depicted in Table VII, we observe that in all cases the correlation times predicted with the SM model are sufficiently greater in comparison with those from the other two models. Also, our model predicts somewhat greater orientational correlation times than the JS model. In any case, the times τ_1^c and τ_2^c are found to be greater than the corresponding times τ_1^b and τ_2^b, respectively. This behavior also becomes obvious from the time evaluation of the ACFs displayed in Fig. 6. Such a feature can be explained in terms of the moments of inertia which correspond to the *b* and *c* principal axes of the molecule. Furthermore, we observe that the Legendre ACFs

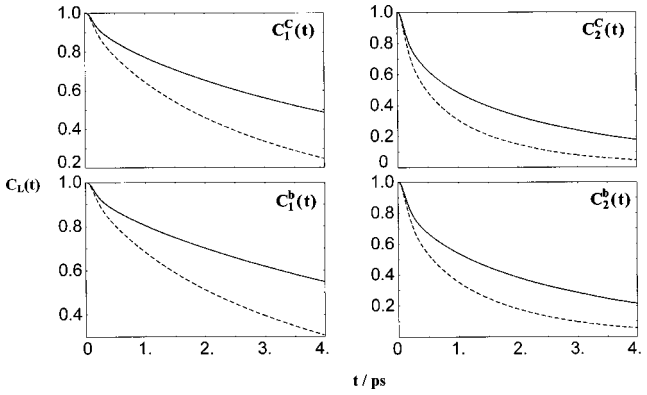

FIG. 7. Temperature dependence of the time autocorrelation functions of the first $C_1^c(t)$, $C_1^b(t)$ and second $C_2^c(t)$, $C_2^b(t)$ order Legendre polynomials of liquid DMF for the CS2 potential model from this MD study (———298 K; – – –373 K).

and their corresponding correlation times show the correct temperature dependence. In Fig. 7 the same quantities are depicted for the CS2 model at both temperatures. The question whether the rotational motion of the DMF molecules in the sample is isotropic has long been a matter of investigation.[15,35,36] The reorientational ACFs and their corresponding correlation times, τ_1^c, τ_1^b, τ_2^c, τ_2^b, appear to be reorientationally anisotropic. The ratio between corresponding τ_1's and τ_2's are an indication for the type of the reorientational diffusion motion. Thus, for a rotational molecular process with relatively small angular steps, the Hubband relation[37] ($\tau_1=3\tau_2$) is fulfilled and the rotational motion can be treated as a diffusional one. Nevertheless, when the rotational motion consists of larger angular steps, the τ_1/τ_2 ratio is expected to be quite smaller than 3. Our data suggest that the rotational motion of the DMF molecules may be characterized as a diffusional one.

We have also attempted to compare our second order reorientational times with those acquired from experimental data. The most appropriate way of precisely assigning the experimental decays to reorientational diffusion about particular molecular axes is sometimes that of NMR techniques. For example, an outstanding technique for the observation of reorientational molecular motion is the one which provides us with the measurements of intramolecular nuclear quadrupole relaxation rates ($1/T_1$) of nuclei with spin $\geqslant 1$ as, e.g., ^{14}N and ^{17}O. Note also that the relaxation rate $1/T_1$ is related to the correlation time τ_2 of the second order Legendre reorientational ACF by

$$\frac{1}{T_1}=\frac{3}{10}\pi^2\left(\frac{2I+3}{I^2(2I-1)}\right)C_{\mathrm{QF}}^2\left(1+\frac{n^2}{3}\right)\tau_C. \tag{8}$$

Here I denotes the nuclear spin quantum number and C_{QF} denotes the nuclear quadrupole coupling constant.

The molecule DMF contains the oxygen and nitrogen atoms, allowing ^{14}N and ^{17}O NMR measurements of the quadrupole relaxation rates of these nuclei. Following the literature, we notice that a number of NMR studies on pure liquid DMF and DMF-d7, as well as on some of their mixtures, have been reported up to now. M. Holz *et al.*[33,38,39] published a series of experimental studies on this system by using the ^{14}N and ^{17}O NMR quadrupole relaxation technique. In Table VII we list the NMR experimental reorientational time $\tau_2=2.4$ ps for liquid DMF at 298 K. From the above results we see that the agreement between NMR τ_2 data and MD simulation with CS2 potential is quite satisfactory. Also, the results from the SM model show the slowest reorientational dynamics, while those from the JS show the fastest ones in comparison with experiment and with the other two model simulations.

Another point of main interest is to explore the dielectric properties of all the aforementioned models for the DMF liquid. In connection to this, however, we shall present here a rather limited discussion of the Debye relaxation time τ_{D} for liquid DMF obtained in the case of the CS2 potential. The complete study of the dielectric properties of the three models of DMF will be reported in a subsequent paper.

The method we have used to obtain the time τ_{D} was based on the accurately determination of the dipole moment ACF $C_M(t)$:

$$C_M(t)=\frac{1}{\langle\vec{M}(0)^2\rangle}\langle\vec{M}(0)\vec{M}(t)\rangle, \tag{9}$$

$$\vec{M}(t)=\sum_{i=l}^{N}\vec{\mu}_i(t). \tag{10}$$

Here $\vec{M}(t)$ is the total dipole moment of the sample at time t and $\vec{\mu}_i(t)$ denotes the permanent dipole moment of the molecule i.

The Debye relaxation time was obtained by means of the relation

$$\tau_{\mathrm{D}}=\frac{1}{\langle\vec{M}(0)^2\rangle}\int_0^\infty\langle\vec{M}(0)\vec{M}(t)\rangle\,dt. \tag{11}$$

We have chosen this method due to the fact that extensive MD studies of model polar fluids,[40,41] using Ewald sums with conducting boundaries, lead to consistent results for the dielectric properties. The success, however, of this method depends thoroughly on the simulation runs which must be long enough to obtain $\langle\vec{M}(0)^2\rangle$ and $C_M(t)$ with reasonable precision. In our case the trajectory used to obtain these properties was of 1 ns long. The $C_M(t)$ function was extrapolated to long times by means of an exponential type function $A\exp(t/\tau)$ and this has been taken into account to obtain the Debye relaxation time. The calculated total dipole ACFs. $C_M(t)$ at 298 and 373 K are shown in Fig. 8. The insert figure corresponds to a previous far infrared experimental study of liquid DMF at 298 K by R. Buchner and J. Yarwood.[42] As we can see, the agreement between the experimental and simulated ACFs $C_M(t)$ at 298 K is excellent. The previous far infrared experiment at 298 K provides a Debye relaxation time τ_{D} of about 13.1 ps (see Table 1 in Ref. 42), which is very close to the estimated MD value $\tau_{\mathrm{D}}=13.2$ ps. Finally, from the shape behavior of the ACF $C_M(t)$ at 373 K and its correlation time $\tau_{\mathrm{D}}=6.8$ ps in comparison with the results at 298 K, we observe a correct temperature dependence of this relaxation process produced in the framework of the present simulation.

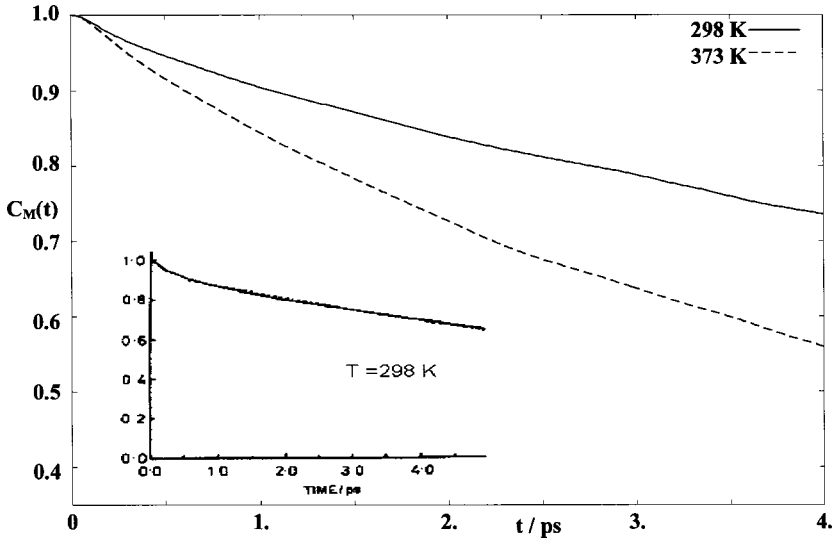

FIG. 8. Total dipole autocorrelation function $C_M(t)$ of liquid DMF from the present MD study at 298 K and 373 K by using our potential model CS2 proposed here. The inset figure corresponds to a previous far infrared experimental study (Ref. 42).

IV. SUMMARY

In the present article, the molecular dynamics technique was employed to simulate the liquid phase of the pure *N*,*N*-dimethylformamide (DMF) using two-body molecular potential models. The simulations were carried out in the NVE and NPT statistical mechanical ensembles at temperatures of 298 and 373 K and at normal pressure.

The focus of this work was to investigate systematically the intermolecular interactions of the liquid. This was achieved by exploring the ability of previously proposed effective potential models in predicting certain properties of the system in the entire temperature range at normal pressure.

In order to realize this, we have performed long simulations of this liquid using the five-interaction site OPLS model due to Jorgensen and Swenson[2] (JS), the six-site potential of Schoester *et al.*[4] (SM), and a six-site potential (CS1) optimized by us in the framework of a recent study.[16] Several properties of these models, including their thermodynamical, structural, transport and some dynamical properties, have been calculated and compared with experimental and previous Monte Carlo data. The present MD results have shown that these models, to a higher or lower degree, provide good descriptions of the system. Specifically, the six-site model CS1 was found to be somewhat superior to the JS model and sufficiently more accurate compared to the SM model regarding the bulk thermodynamical properties of the liquid. However, the comparison with some experimental dynamical properties has shown that a slightly further improvement of the parameter of the CS1 potential is needed in order to improve agreement with experimental data. This has been done on the basis of a simple but very time consuming scaling reparametrization procedure, and a new six-interaction site OPLS computational model (CS2) was developed.

After further testing, the present OPLS model CS2 was shown to yield the most successful results in comparison to the other models, not only regarding the bulk thermodynamical properties but also the reorientational and the Debye rotational relaxation times, as well as the self-diffusion and the shear viscosity coefficients of the liquid.

ACKNOWLEDGMENTS

This work was carried out within the project No. 70/4/3349AU. The financial support of the University of Athens is gratefully acknowledged. The CPU time allocation on CONVEX C3820 and on HP 735 (eight nodes) of the Computing Center of the University of Athens, Greece, is also gratefully acknowledged.

[1] S. Yashonath and C. N. R. Rao, Chem. Phys. **155**, 351 (1991).
[2] W. L. Jorgensen and C. J. Swenson, J. Am. Chem. Soc. **107**, 569 (1985).
[3] J. W. Essex and W. L. Jorgensen, J. Phys. Chem. **99**, 17956 (1995).
[4] P. C. Schoester, M. D. Zeidler, T. Radnai, and P. A. Bopp, Z. Naturforsch., **50**, 38 (1995).
[5] E. D. Schmid and E. Brodbek, J. Mol. Struct. **108**, 17 (1984); P. Schoester, Thesis, RWTH Aachen Germany, 1995.
[6] H. Ohtaki, S. Itoh, T. Yamaguchi, S. Ishiguro, and B. M. Rode, Bull. Chem. Soc. Jpn. **56**, 3406 (1983).
[7] T. Radnai, S. Itoh, and H. Ohtaki, Bull. Chem. Soc. Jpn. **61**, 3845 (1988).
[8] J. Gao, J. J. Parelites, and D. Habibollazadeh, J. Phys. Chem. **100**, 2689 (1996).
[9] J. Gao, J. Am. Chem. Soc. **115**, 2930 (1993).
[10] J. Gao, D. Habibollazadeh, and L. Shao, J. Phys. Chem. **99**, 16460 (1995).
[11] Y. Ding, D. N. Bernardo, K. Krogh-Jespersen, and R. M. Levy, J. Phys. Chem. **99**, 11575 (1995).
[12] A. Wallqvist and B. J. Berne, J. Phys. Chem. **97**, 13841 (1993).
[13] A. H. de Vries, P. Th. Van Duijen, A. H. Suffer, J. A. C. Rullmann, J. P. Dijkman, H. Merenga, and B. T. Thole, J. Comput. Chem. **16**, 37 (1995).
[14] H. Nakanishi and O. Yamamoto, Chem. Phys. Lett. **35**, 407 (1975).
[15] R. Konrat and S. H. Sterk, J. Phys. Chem. **94**, 1291 (1990).
[16] M. Chalaris and J. Samios, J. Mol. Liq. **78**, 201 (1998).
[17] E. Benedetti, in *Proceeding of the Fifth American Peptide Symposium*, edited by M. Goodman and J. Meinhofer (Wiley, New York, 1977), p. 27.
[18] G. Schultz and I. Hatzittai, J. Phys. Chem. **97**, 4966 (1993).
[19] X. Zhou, J. A. Krauser, D. R. Tato, A. S. VanBuren, J. A. Clark, P. R. Mody, and R. Lim, J. Phys. Chem. **100**, 16822 (1996).
[20] W. L. Jorgensen, J. Chandrasekhar, J. D. Madura, R. W. Impey, and M. L. Klein, J. Chem. Phys. **79**, 926 (1983).
[21] W. L. Jorgensen, J. D. Madura, and C. J. Swenson, J. Am. Chem. Soc. **106**, 6638 (1984).
[22] J. Samios, D. Dellis, and H. Stassen, Chem. Phys. **178**, 83 (1993).
[23] A. Luzar, A. K. Soper, and D. Chandler, J. Chem. Phys. **99**, 6836 (1993).
[24] H. Liu, F. M. Plathe, and W. F. van Gusteren, J. Am. Chem. Soc. **117**, 4363 (1995).
[25] J. F. Yan, F. A. Momary, R. Hoffmann, and H. A. Scheraga, J. Phys. Chem. **74**, 420 (1970).
[26] A. T. Hangler, E. Huller, and S. Lifson, J. Am. Chem. Soc. **96**, 5319 (1974).

[27] V. S. Dimitrov and J. A. Ladd, J. Mol. Struct. **159**, 107 (1987).
[28] D. Steele and A. Quatermain, Spectrochim. Acta A **43**, 681 (1987).
[29] J. Richardi, Thesis, Regensburg, Germany, 1996.
[30] S. Yasonath, S. Price, and I. R. Mc Donald, Mol. Phys. **64**, 361 (1988).
[31] G. Marechal and J. P. Ryckaert, Chem. Phys. Lett. **101**, 548 (1983).
[32] D. J. Evans and W. B. Street, Mol. Phys. **36**, 161 (1978); G. Marechal, J. P. Ryckaert, and A. Bellemans, *ibid.* **61**, 33 (1987).
[33] M. Holz, X. Mao, D. Seiferling, and A. Sacco, J. Chem. Phys. **104**, 669 (1996).
[34] R. M. Lynden-Bell and W. A. Stelle, J. Phys. Chem. **88**, 6514 (1984).
[35] R. Rodriquez and J. L. McHale, J. Phys. Chem. **88**, 2273 (1988).
[36] Y. J. Chang and E. W. Castner, J. Phys. Chem. **98**, 9712 (1994).
[37] P. S. Hubbard, Phys. Rev. **131**, 1155 (1963).
[38] H. Weingaertner, M. Holz, and H. G. Hertz, J. Solution Chem. **7**, 689 (1978).
[39] X. Mao and M. Holz, Z. Naturforsch., **49**, 1016 (1994).
[40] M. Neumann, J. Chem. Phys. **82**, 5663 (1985).
[41] M. G. Kurnikova, N. Balabai, D. H. Waldeck, and R. D. Coalson, J. Am. Chem. Soc. **120**, 6121 (1998).
[42] R. Buchner and J. Yarwood, Mol. Phys. **71**, 65 (1990).